Analysis of Radiative Mantle Formation by Impurity Seeding in ITER

Ikuhiro YAMADA, Kozo YAMAZAKI, Tetsutarou OISHI, Hideki ARIMOTO and Tatsuo SHOJI

Department of Energy Engineering and Science, Nagoya University, Furo-cho, Chikusa-ku, Nagoya 464-8603 Japan

(Received 9 December 2009 / Accepted 7 May 2010)

In order to reduce high heat load on divertor plate in fusion reactors, we investigated radiative mantle formation scenarios by impurity seeding into scrape off layer (SOL) in ITER using the TOTAL simulation code. The low-*Z* impurity, like He, could not form a radiative mantle and have almost no contribution to the reduction of divertor heat load. On the contrary, the medium-*Z* impurity, like Kr, can form radiative mantle definitely and can radiate about 84% (core:33% / mantle:51%) of input power inside the last closed flux surface (LCFS) without any serious changes in density and temperature profile, and without inducing back transition from H to L mode. It can reduce divertor heat load about 60% compared with the case of no impurity injection in ITER.

Keywords: impurity, transport, radiative mantle, divertor, ITER

DOI: 10.1585/pfr.5.S2033

1. Introduction

Unacceptably large power flux exhausted to the divertor region is one of the most serious issues in ITER. In particular, for future fusion reactors, heat loads on divertor plates are predicted to be very large, and therefore, plasma facing component materials would not tolerate their heat load.

To this problem, two different methods reducing heat load on divertor plates have been proposed. One is the solution called ‘radiative divertor’, and the other is ‘radiative mantle’.

In former solution, impurities are seeded into divertor chamber, and corresponding radiation enhancement is occurred inside the divertor region. On the other hand, in the latter one, impurities are seeded into scrape off layer (SOL) and convert the high energy flux into line radiation near the plasma edge which can scatter over the wider surface area of the first wall and divertor chamber.

If the radiative mantle formation could be maintained without inducing any harmful effects, it would be a beneficial solution to heat load problem in thr next generation reactor.

In this analysis, we investigated radiative mantle formation by impurity seeding in ITER device. The radial distribution of impurity ions is calculated by using a 1.5-dimensional (1.5-D) toroidal transport analysis linkage code (TOTAL) [1]. In Section 2, the simulation code used in this paper is described. In Section 3, simulation results are presented, and a summary and discussions are presented in Section 4.

author’s e-mail: yamazaki@ees.nagoya-u.ac.jp

2. Numerical Model

2.1 Transport model

To investigate transport of fuel and impurity ions in a tokamak, we used a 1.5-D (1-D transport/2-D equilibrium for tokamak) time-dependent simulation model with low-*Z* gas and high-*Z* metal impurity dynamics. The plasma density n_e, n_i and temperature T_e, T_i are described as follows.

$$\frac{\partial n_e}{\partial t} + \frac{1}{V'}\frac{\partial}{\partial \rho} V'\Gamma_e = S_P, \tag{1}$$

$$\sum_i z_i n_i \approx n_e, \tag{2}$$

$$\frac{3}{2}\frac{\partial n_e T_e}{\partial t} + \frac{1}{V'}\frac{\partial}{\partial \rho}\left\{V'\left(q_e + \frac{5}{2}\Gamma_e T_e\right)\right\} = P_{He} - P_{ei} - P_{rad} - \Gamma_e E_r, \tag{3}$$

$$\frac{3}{2}\frac{\partial n_i T_i}{\partial t} + \frac{1}{V'}\frac{\partial}{\partial \rho}\left\{V'\left(q_i + \frac{5}{2}\Gamma_i T_i\right)\right\} = P_{Hi} - P_{ei} - P_{cx} - z_i\Gamma_i E_r, \tag{4}$$

where q_e and q_i are electron and ion thermal energy fluxes, P_{He} and P_{Hi} are additional electron and ion heating powers, P_{ei} is equi-partition power, P_{rad} and P_{CX} are radiation and charge-exchange loss powers, respectively. Here, ρ is the normalized radius, V is the volume defined by the equilibrium magnetic surface and its derivative is defined by $V' = dV/d\rho$. The radiation loss P_{rad} is the sum of bremsstrahlung radiation, impurity line radiation, and synchrotron radiation powers.

For the anomalous part of the transport coefficients, the scaling model is used in this paper.

$$\chi_{ano} = \chi_0(t)(1 + \lambda\rho^{\mu}), \tag{5}$$

$$\chi_0(t) = \chi_0(t - \Delta t) + \Delta\chi\left(\tau_E^{pla}/\tau_E^{SC} - 1\right). \tag{6}$$

A simple parabolic profile ($\mu = 2$) and $\lambda \equiv \chi_a/\chi_0 - 1 = 1$ model is assumed for the thermal transport coefficient. Here, τ_e^{pla} is global energy confinement time calculated from the global plasma energy and the total heating power. For the scaling global confinement time τ_E^{SC}, we use the following L- and H-mode scaling laws,

$$\tau_E^{ITER-P}(s) = 0.048 I_P^{0.85} R^{1.2} \times a^{0.3} n_{20}^{-0.1} B^{0.2} (A_i \kappa_s / P)^{1/2}, \tag{7}$$

$$\tau_E^{IPB98y2}(s) = 0.0562 I_P^{0.98} B_t^{0.15} \times P^{-0.69} M_i^{0.19} R^{1.97} n_{e19}^{-0.41} \varepsilon^{0.58} \kappa^{0.87}. \tag{8}$$

Using this model, we can simulate most probable plasma confinement derived from various experimental machines.

2.2 Impurity model

We examined impurities with a model for impurities in TOTAL; the multi-species dynamic impurity code IMPDYN [3] was used to model the ionization states, and the NCLASS code [4] was used for the full neoclassical transport of each charge state considering arbitrary aspect ratio and collisionality.

For the impurity dynamics [5,6], the rate equation and diffusion equation are solved using the IMPDYN code [3] coupled with the ADPAK atomic physics package [7], which can calculate the cooling rate,

$$\frac{\partial n_k}{\partial t} = -\frac{1}{V'}\frac{\partial}{\partial \rho}(V'\Gamma_k) + [\gamma_{k-1} n_{k-1} + \alpha_{k+1} n_{k+1} - (\gamma_k + \alpha_k) n_k] n_e + S_k, \tag{9}$$

$$\Gamma_k = \Gamma_k^{NCs} + \Gamma_k^{NCa} - D_k(\rho)\frac{\partial n_k}{\partial \rho} + V_k(\rho) n_k. \tag{10}$$

with ionization rate γ_k, recombination rate α_k, and impurity source term S_k. Here a constant anomalous diffusion coefficient D_k and simply modeled inward velocity $V_k = V(a)(r/a)$ are used for impurity anomalous transport ($V_k < 0$ corresponds to inward velocity). The main fuel neutrals are calculated by the AURORA Monte Carlo code [8].

The neoclassical impurity flux in a tokamak is expressed by

$$\Gamma_k^{NCs} = -D_k^{NC}\nabla n_k + D_k^{NC} n_k \left[\sum_{l\neq k}(g_{nl\to k}\nabla n_l / n_l) + g_{Ti}\nabla T_i / T_i + g_{Te}\nabla T_e / T_e\right]. \tag{11}$$

In the simulation, the impurity source was defined as the impurity neutral flux on the plasma boundary. The neutral impurity density profile $n_0(\rho)$ is assumed to be

$$n_0(\rho) = -\frac{V'(1)\Gamma_0(1)}{V'(\rho)\nu_0}\exp\left(-\frac{1}{\nu_0}\int_1^\rho d\rho n_e(\rho)\gamma_0(\rho)\right), \tag{12}$$

derived from

$$\frac{\partial n_0}{\partial t} = -\frac{1}{V'}\frac{\partial}{\partial \rho}(V'\Gamma_0) - \gamma_0 n_e n_0 \approx 0, \tag{13}$$

$$\Gamma_0(\rho) \approx -n_0(\rho)\nu_0. \tag{14}$$

Here, $\Gamma_0(1)$ is the neutral impurity flux at the plasma boundary ($\rho = 1$), and ν_0 is the neutral impurity inward velocity (assuming an energy of 10 eV). The symbols γ_0 and n_e are the ionization coefficient and electron density near the plasma boundary, respectively.

To clarify the effect of impurity ions, steady-state burning plasma conditions were established without impurities. Then, a continuous neutral impurity influx was introduced, and after a transient phase, the system settled into a new radiation-enhanced steady state.

2.3 Divertor model

In this analysis, two point model based on Borrass model [9] is coupled to the TOTAL code.

$$n_D = \frac{f_P}{1 + M_D^2}\frac{n_S T_S}{T_D}, \tag{15}$$

$$\Delta = \frac{5}{32}\frac{c}{e}\frac{n_S T_S^2 F}{q_\perp B_t}, \tag{16}$$

$$T_S = \left(\frac{49}{4\kappa}\frac{q_\perp L^2}{\Delta}\right)^{2/7}, \tag{17}$$

$$\frac{7}{2}\frac{L\left(1 - f_{imp}\right) q_\perp}{\Delta} = c_s n_D M_D \left[\xi + \left(\gamma' + M_D^2\right) T_D\right]. \tag{18}$$

Here, subscripts S and D represent stagnation point and divertor quantities, respectively. L is the connection length and $q_\perp$ is the mean power flux across the separatrix. M_D is the Mach number at the target. The coefficient f_p is the drop of total pressure (static and kinetic by momentum loss due to ion-neutral collisions) in the divertor region and we use $f_p = 2$ as an input parameter in this simulation. The coefficient f_{imp} is the impurity radiative fraction in the SOL region and is assumed $f_{imp} = 0$ in this analysis. Therefore we did not include the impurity radiation in the SOL region.

3. Simulation Results

3.1 Maximum impurity concentration

We investigated radiative mantle formation in ITER for low-Z impurity (He, C, O, Ne) and medium-Z impurity (Ar, Fe, Kr, Mo). To clarify the maximum impurity concentration at the reference ITER inductive scenario based on the ELMy H-mode regime, we use the following three constraints.

$$P'_\alpha - P_\alpha \leq P_\alpha \cdot 5\%, \tag{19}$$

$$\bar{P}_{fus} \geq 10\bar{P}_{RF}, \tag{20}$$

$$P_{sep} \geq P_{H\to L}. \tag{21}$$

Here, P_α and P'_α are the alpha power before and after impurity injection. These simulation results are presented in

Table 1 Related parameters for various impurity species at maximum concentration.

	No imp	He	Ne	Ar	Kr
f_{imp} [%]	0	11.543	0.9729	0.1707	0.0166
P_{rad} [MW]	26.75	66.35	105.7	115.92	132.51
P_{sep} [MW]	130	85.94	51.11	41.79	25.87
$P_{H\rightarrow L}$ [MW]	25.08	85.94	27.66	25.82	25.04
T_{es} [eV]	185.31	149.1	132.91	126.12	111.85

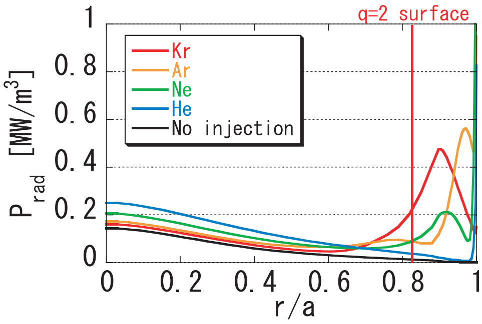

Fig. 1 Radiation power density profile for different impurity species at maximum concentrations.

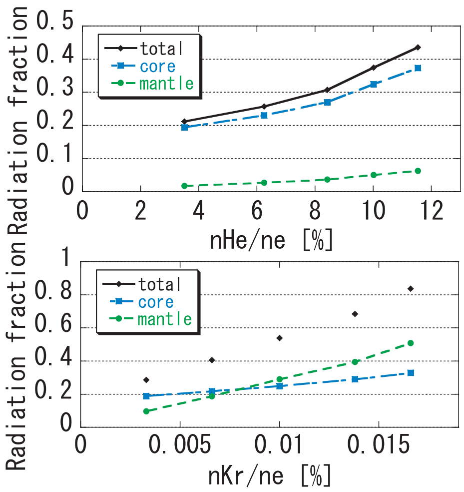

Fig. 2 Radiation fraction versus impurity concentration.

Table 1, and Figure 1 shows that the radial profile of total radiation power for various impurity species at maximum concentration in Table 1.

3.2 Impurity dependence of radiation fraction

Figure 2 shows the radiation fraction dependence on impurity concentration for the case of injecting He, Ne, Ar and Kr. Here, we define the region between $q = 2$ surface and LCFS as plasma mantle region, and assume the region inside the $q = 2$ surface as plasma core region. In the case of He injection, the ratio of radiation from the core increases rather than those from the mantle region as

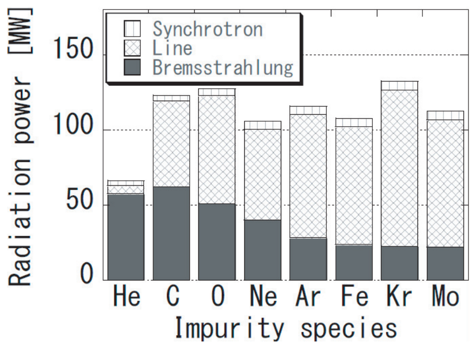

Fig. 3 Total radiation for each impurity species.

impurity concentration increases. On the contrary, in Kr injection case, the ratio of the mantle radiation to the total radiation exceeds that of the core radiation at about Kr concentration of 0.008% with respect to electron density. As shown in the figure, Kr impurity can form radiative mantle definitely, and radiate about 51% of input power from the mantle, and 33% from the core.

3.3 Total exhausted radiation

The ratio of each radiation process (bremsstrahlung radiation, impurity line radiation, and synchrotron radiation) on total radiation is summarized on bar chart in Figure 3. The injected Kr impurity is the most radiative by the line radiation near the plasma edge, and the impurity density is rather small, which is keeping bremsstrahlung radiation loss to the lower level. In the case of He impurity, injected impurity is almost all ionized in the core, even near the edge, and the impurity density is several hundred times larger than that of Kr impurity case. Therefore, it induces the increase in effective-Z, and correspondingly causes large bremsstrahlung radiation loss rate.

3.4 The case of Kr injection

In previous subsections, we clarified that Kr impurity can form radiative mantle. Thus, we confirm whether any deleterious changes are induced after Kr impurity injection in this subsection.

The time history of global power quantities are shown in Figure 4. The Kr impurity injection is started at t = 100 sec, and simultaneously power flux across the separatrix P_{sep} is reduced a lot. Through impurity injection, alpha heating power P_{alp} is feedback controlled to keep 105 MW by fuel gas puffing. In Fig. 5, the contours of Kr impurity density and corresponding total radiation profile are shown. They represent that impurity radial profile and corresponding radiation mantle is settled to the steady state at 30 sec after starting of impurity injection.

Figure 6 shows the radial profiles of electron density, electron temperature and ion temperature before and after impurity injection. The electron density is increased and the temperature profile becomes slightly peaked through impurity injection. After impurity injection, the effective

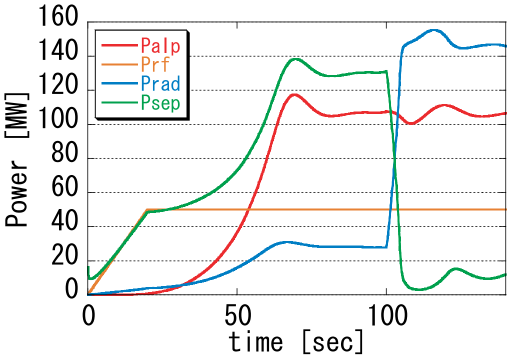

Fig. 4 Time history of global power balance quantities. Kr impurity injection starts at t = 100 sec.

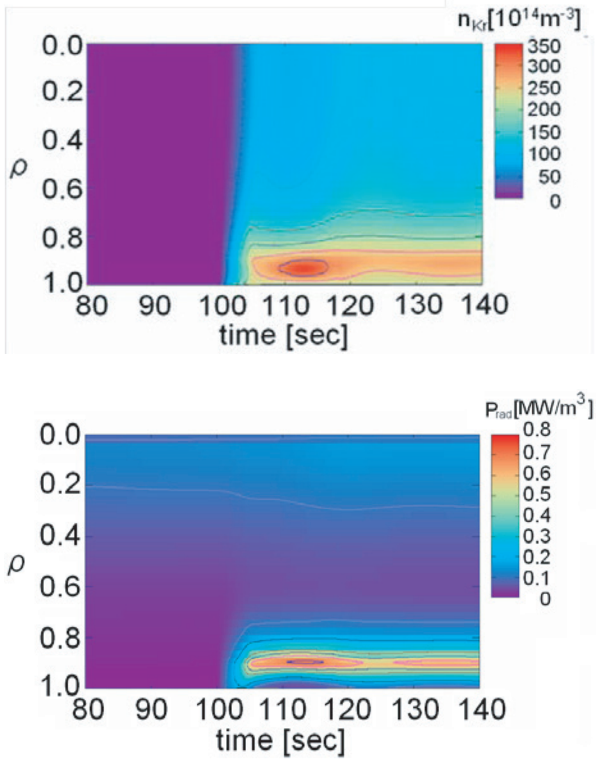

Fig. 5 Contours of Kr impurity density (upper graph) and radiation power (lower graph) for ρ and time.

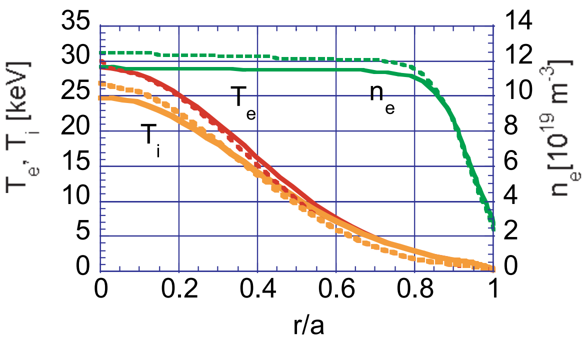

Fig. 6 Radial profile of electron density, electron temperature and ion temperature before (solid line) and after (dashed line) impurity injection.

Z changes from 1.65 to 1.83. The current profile does not change so much. The critical changes in other plasma parameters could not be obtained without back transition from H to L mode.

4. Summary and Discussions

We investigated radiative mantle formation by impurity seeding in ITER and clarified the following results:

(1) Low-Z impurity, like He, cannot form radiative mantle, and causes large bremsstrahlung radiation loss in the core.

(2) About 84% (core:33% / mantle:51%) of input power is radiated inside the LCFS by Kr impurity seeding without inducing any deleterious change.

The deference between the radiative mantle formation by Kr and by He seems to come from the atomic processes including ionization, recombination and their relevant radiation processes. The impurity transport processes including inward flows are also generally important, but these effects on the difference might be small in the present parabolic transport coefficient model derived from the global confinement scaling law.

In this simulation, impurity transport in SOL/divertor region is not included and impurity influx is supposed at LCFS. In the case of low-Z impurity, almost all impurity atoms injected into the plasma periphery might be ionized in SOL. However, high-Z impurities such as tungsten impurities will penetrate into the core as partially ionized particles. That high-Z impurity penetration process was calculated in this simulation as shown in Ref. [6]. We should also consider the case of impurity pellet injection. The detailed dynamics of impurity neutrals including ionization and recombination requires 3-dimensional simulation, which is out of scope in the present research The impurity total analysis from the core to the divertor region is needed, and we will discuss the relation between radiative mantle and ‘radiative divertor’ in the near future.

[1] K. Yamazaki and T. Amano, Nucl. Fusion **32**, 633 (1992).
[2] A. Taroni *et al.*, Plasma Phys. Control. Fusion **36**, 1629 (1994).
[3] T. Amano, J. Mizuno and J. Kako, ‘Simulation of Impurity Transport in Tokamak’, Internal report IPPJ-616, Institute of Plasma Physics, Nagoya Univ. (1982).
[4] W. A. Houlberg *et al.*, Phys. Plasma **4**, 3230 (1997).
[5] Y. Murakami, T. Amano *et al.*, J. Nucl. Material **313-316**, 1161 (2003).
[6] K. Yamazaki *et al.*, J. Plasma Fusion Res. SERIES **7**, 102 (2006).
[7] R. A. Hulse, Nucl. Technol. Fusion **3**, 259 (1983).
[8] M. H. Huges and D. E. Post, J. Compt. Phys. **28**, 43 (1978).
[9] K. Borrass *et al.*, Nucl. Fusion **31**, 1035 (1991).